Theoretical Study of a Mission Adaptive Wing

André Luiz Martins
Fernando Martini Catalano
Aircraft Laboratory - USP - Brazil

ABSTRACT

A theoretical preliminary study to evaluate the aerodynamic performance of a chordwise elastically deformable transport aircraft wing has been performed. The study has been concentrated on the potential use of such wing to reduce induced drag during takeoff and climb and on its performance to produce high lift for landing. As a reference, similar analysis have been made for a conventional wing of same planform, equipped with modern high lift devices. To perform the evaluations, a constrained direct optimisation method has been used, composed of a vortex lattice analysis method coupled to a multivariable function minimiser algorithm. To produce basic deformation solutions with minimum structural feasability guidelines, a linear finite element method for flat plates have been used. Within the limitations and simplified modelling assumed for this preliminary study, it has been concluded that no great induced drag reductions may be expected over typical transport aircraft wing designs. Also, to have high lift performance comparable to conventional current wing designs, deformable camber airfoil wing sections must have maximum lift coefficients much higher than equivalent airfoils with plain leading and trailing edge flaps.

List of Symbols

x, y, z	Reference coordinate system (Fig. 1)
g	Gravity acceleration (9.81 m/s^2);
m	Aircraft mass (kg);
ρ	Air density (kg/m^3);
U_∞	Freestream flow velocity (m/s);
M	Mach number;
b	Wing span (m);
mac	Mean aerodynamic chord (m);
c(y)	Spanwise chord distribution (m);
c_{root}	Wing root chord (m);
c_{tip}	Wing tip chord (m);
λ	Wing taper ratio, c_{tip}/c_{root};
S	Reference area (projected wing area - m^2);
α	Aircraft angle of attack (degrees);
δ_f	(Equivalent) flap deflection (degrees);
L	lift force (N);
Di	induced drag force (N);
C_L	Lift coefficient, $L/(\frac{1}{2}\rho U_\infty^2 S)$;
C_{Di}	Induced drag coefficient, $D_i/(\frac{1}{2}\rho U_\infty^2 S)$;
$l(y)$	Spanwise non-dimensional lift distribution;
$c_l(y)$	Spanwise lift coefficient distribution;
$c_{lb}(y)$	Spanwise basic lift coefficient distribution;
$c_{la}(y)$	Spanwise additional lift coefficient dist.;
$c_{lpmax}(y)$	Spanwise airfoil maximum lift coefficient dist.;
$\{X_i\}$	Optimisation decision variables set;
$F(\{X_i\})$	Optimisation objective function;
$\{W_{iTE}\}$	Trailing edge deformation basic solutions;
$\{W_{iTE}\}$	Leading edge deformation basic solutions;
$\{P_{iTE}\}$	Trailing edge deformation linear combination parameters;
$\{P_{iTE}\}$	Leading edge deformation linear combination parameters;
E	Material elasticity modulus (N/m);
υ	Material Poisson coefficient;
t	Flat plate thickness (m);

Subscripts

max	maximum;
opt	optimum;
TE	Trailing edge;
LE	Leading edge;

Prefixes

Δ	variation;

Introduction

Throughout the last four decades, several schemes have been envisaged to make aircraft geometry variation a viable proposal for better mission adaptation[1]. Some of them reached practical feasability, such as variable sweep wings or, on a simpler level, complex high lift devices configurations.

One of the possibilities that have been considered (theoretically and experimentally) is geometrical adaptation of wings by elastic deformation. Through such scheme, the greatest benefits could come from suitable airfoil camber smooth spanwise variation to adequate the aircraft to each of its flight phases, both by better enhancement of local airfoil performance and by adequation of wing spanwise lift distribution.

Although some successes have been achieved to design a feasible elastically deformable wing by active intervention (ex.: NASA's variable camber wing F-111), it is needless to mention that to make the concept possible for practical use would be a far more complex and extensive task. First of all, feasability studies should be made referring to numerous disciplines, such as aeroelasticity, structural fatigue, materials, maintenance and many others. Above

all, the real aerodynamic benefits that could be reached must be evaluated.

Within that context, a preliminary evaluation of the potential benefits of a variable camber transport aircraft wing have been made, in respect to induced drag reduction for various flight conditions and the use of variable camber to produce high lift. A computational optimisation method and simple finite element analysis method have been used. Results were compared with a typical modern transport aircraft wing design with high lift devices.

Definition of Case Study and Methods Used

To perform this study, typical configuration and flight conditions for a modern transport aircraft wing has been considered. The planform geometry chosen (considering no deformation) is shown in Figure 1(a).

Based on previous proposals found in literature, a typical wing section geometrical deformation scheme has been devised in which the centre section is fixed, working as the main loading carrying wing box. Both trailing and leading edges are elastically deformable to a certain extent of the chord, namely between 0 and 20% of the chord and between 70 and 100% of the chord. Figure 2 brings an schematic illustration of the concept on a modern supercritical airfoil.

For this work it has been supposed that such figures would be extended to the whole wingspan (Figure 3). As mentioned above, a comparative study has been performed in relation to a flapped wing. For the sake of simplicity it has been supposed that such flap would be full span and occupying 25% of the wing chord.

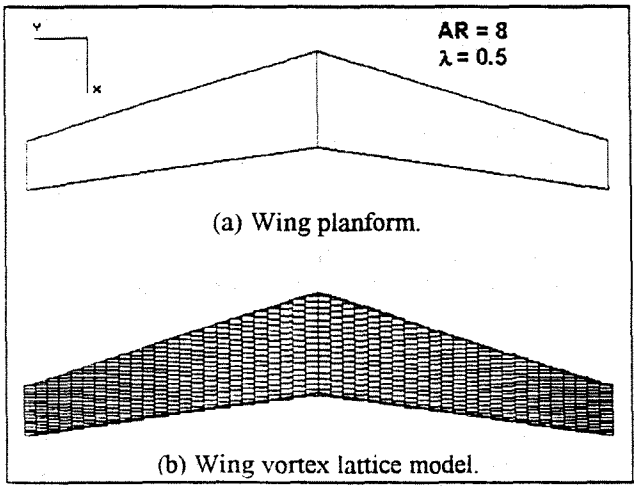

(a) Wing planform.

(b) Wing vortex lattice model.

Figure 1 - Transport aircraft wing configuration.

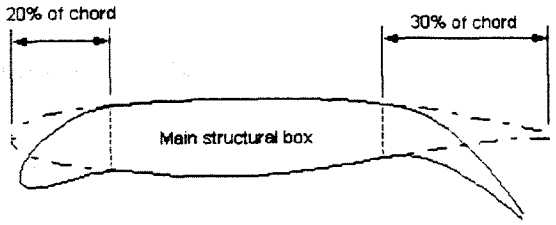

Figure 2 - Variable camber wing section.

Structural Deformation Model

It is obvious that the feasability of intentional, large magnitude wing elastic deformation would depend on many influent factors, such as materials employed and structure configuration. Also, to determine how such structure would deform and if given desired deformation states are possible or not requires, at least, extensive and complex non-linear finite element analysis.

Once this work focuses on preliminary evaluation, such analysis are out of scope. On the other hand, deformation models able to give minimum structural feasability guidelines are required, once it is useless to determine only aerodynamically ideal deformations.

Given this problem, a first order simplification considered of interest is to represent the deformation of the mean surface of the deformable regions of the wing by that of thin plates of same planform and with a reasonable equivalent thickness. From that hypothesis, a simple linear finite element method for thin flat plates[2] has been adopted to determine deformation states with minimum feasability. The method is able to give results for small deformations, treating generic quadrilateral plates discretized in regularly spaced elements. The finite element model used for both leading and trailing edge deformable regions is shown in Figure 3.

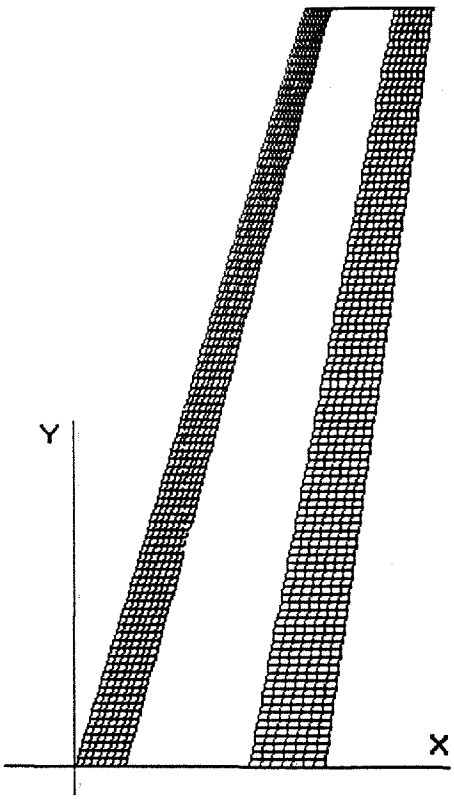

Figure 3 - Wing deformable areas finite element model (half wing shown).

From linear flat plates deformation theory, it can be verified that deformation is proportional to the plate rigidity given by[3]:

$$D = \frac{Et^3}{12\left(1-\upsilon^2\right)} \qquad (1)$$

Linear flat plat deformation differential equations involve only υ, the material's Poisson coefficient. It has been assumed a value of $\upsilon = 0.3$ for all the cases. Given arbitrary values of E and t, fictitious load values can be worked on to produce a certain amount of deformation.

Without any proposal for an active mechanism able to produce a desired wing deformation, it has been supposed that a superlative extrapolation for an ideal mechanism is one able to load the wing's deformable areas uniformly and in a direction normal to the areas. Also, the loading has been figured out to be applied directly to the trailing and leading edge lines. Once results from linear finite element analysis can be linearly combined, a set of six basic "unitary height" distributed triangular loading has been analysed, three for the leading and three for the trailing edge; intermediary desired deformations could be obtained by linear combination of those basic solutions. The set of basic loadings adopted is shown if Figure 4. The resulting basic solutions are shown in Figure 5, as the vertical displacement of the trailing and leading edge lines.

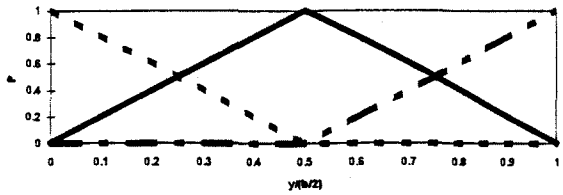

Figure 4 - Set of basic "unitary height" downward triangular distributed loadings (same for leading and trailing edge).

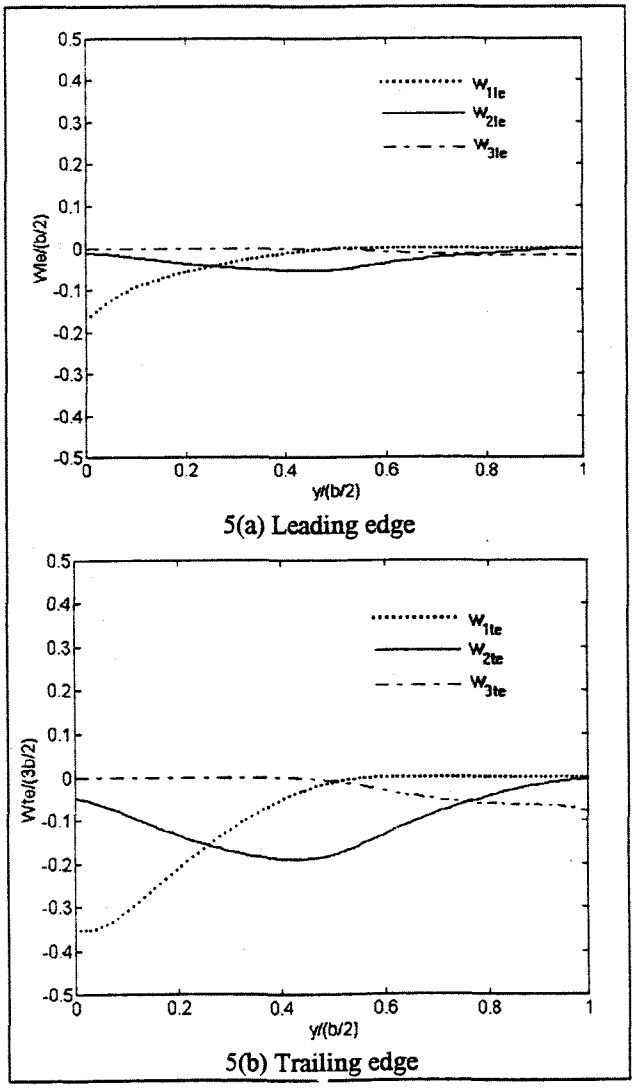

Figure 5 - Basic finite element solutions obtained for the basic loadings (only the leading and trailing edge lines vertical displacements are shown).

Although the eventually large deformations mentioned in this work are obviously out of linear, small deformation hypothesis, the linear results have been extrapolated and used, once they were the best first approximation

available and were compatible with the complexity necessary for a first evaluation.

Aerodynamic Analysis and Optimisation Method

An aerodynamic computational constrained optimisation method has been used to determine the best possible deformed wing configurations at given flight conditions. Such method is composed by a 3D vortex lattice analysis method for lifting surfaces coupled to a multi-variable function optimiser algorithm[4] (*).

The vortex lattice method (VLM)[4] (*) is a numerical solution of the lifting surface theory equations for inviscid potential flow. The real lifting surfaces are approximated by a set of trapezoidal planar elements, with no thickness taken into account. Figure 1(b) presents the VLM discretized model used for the typical wing configuration. Although less sophisticated than higher order panel methods, the VLM is capable of great prediction accuracy for global forces and lift distributions of free lifting surfaces. It is very adequate for preliminary design needs and has low computational cost, reasons that make it ideal for this preliminary evaluation.

The optimiser algorithm is able to use the VLM as a multivariable function evaluator, in which a chosen objective aerodynamic characteristic F (for example, induced drag) is dependent of a given set of decision variables $\{X_i\}$ (for example, geometric characteri tics). The optimiser is then able to numerically search for the set of decision variables values $\{X_i\}_{opt}$ which returns the minimum (or maximum) value of the objective aerodynamic characteristic chosen $F(\{X_i\}_{opt})$, in an iterative process of analysis and evaluation. The final set of decision variables must be constrained to a certain domain, to ensure that the final result is feasible for the mission required.

In this case study, the decision variables are the coefficients $\{P_{iLE}\}$ and $\{P_{iTE}\}$ in the linear combination equation involving all the six basic deformation solutions (Figure 5). Given this, the vertical displacement of a certain point on the mean surface of the leading edge deformable area of the wing can be represented by:

$$W_{LE} = W_{1LE}\,P_{1LE} + W_{2LE}\,P_{2LE} + W_{3LE}\,P_{3LE} \quad (2a)$$

For a point on the trailing edge region:

$$W_{TE} = W_{1TE}\,P_{1TE} + W_{2TE}\,P_{2TE} + W_{3TE}\,P_{3TE} \quad (2b)$$

The values $\{W_{iTE}\}$ and $\{W_{iTE}\}$ are the vertical displacements determined for the point in question by the basic solutions for the trailing and leading edges respectively.

Once the deformation is defined in this way, chordwise camber angles distributions can be determined for each spanwise station and can be included in the vortex lattice analysis. Such inclusion is made only by modification of contour conditions[4] by the local chordwise camber angles, so that the real deformed configuration is not directly taken into account. These analysis conditions have been considered sufficient for this preliminary evaluation.

Aircraft Mission Conditions and Objectives

Once the structural model, aerodynamic analysis and optimisation conditions have been established, typical transport aircraft mission requirements and objectives have been defined as guidelines for the case study[5]. The following main points can be mentioned:

(a) During takeoff and initial climb, lift to drag ratios determine maximum takeoff lengths and climb rates. Typical lift coefficient values are C_L = 1.2 to 1.7. Also, angle of attack α is limited either by ground clearance or by excessive increase in overall pressure drag.

(b) In cruise flight, the greatest contributions to overall drag come from viscous friction and compressibility effects. Nevertheless, beneficial induced drag reductions could be attained without greatly influencing the other drag sources, by suitable lift distribution shaping.

(c) During landing, large maximum lift coefficients are necessary, ranging from C_L = 2.8 to 3.5, to reduce landing speeds. No minimum drag requirement is made (within the limitations of the powerplant), once steep and slow glide paths are desirable.

From these guidelines, the following study sequence has been envisaged as ideal:

(i) To determine, through constrained optimisation, the minimum induced drag values possible for C_L values ranging from 0.2 to 1.4. These values are representative for the takeoff, climb and cruise, when minimum drag is desirable. Also, the angle of attack is constrained to a maximum of 6° due to conditions mentioned in item (a) above. The same process is performed for a flapped wing.

(ii) To determine, through constrained optimisation, the wing deformed configuration which produces the maximum lift coefficient C_{Lmax} possible. The same process is performed for a flapped wing.

(*) Reference 4 has also been published at ICAS 96 (Aerodynamics II - Student Session) and explains the analysis and optimisation methods in deeper detail.

Wing C_{Lmax} determination

Item (ii) above requires a feasible procedure to determine C_{Lmax} produced by the wing. To evaluate it, the classical method[4],[7] of extrapolation of the spanwise lift coefficient distribution $c_l(y)$ to C_{Lmax} has been used. In that method, the $c_l(y)$ distribution is assumed to have a linear relation wit C_L, even near the stall angle of attack, of the form:

$$c_l(y) = c_{lb}(y) + C_L c_{la}(y) \tag{3}$$

From that point it can also be stated that is C_{Lmax} is reached when the local lift coefficient $c_l(y)$ first reaches the local maximum profile lift coefficient $c_{lpmax}(y)$. From this statement and Equation (3), the following can be written:

$$C_{Lmax} = \min\left(\frac{c_{lpmax}(y) - c_{lb}(y)}{c_{la}(y)}\right) \tag{4}$$

Although seemingly crude, method can be very precise for high aspect ratio surfaces[7], using the linear results from the VLM, and is sufficient within the scope of this work.

The formulation described above also requires the values of the $c_{lpmax}(y)$ spanwise distribution. This distribution is a function of flap deflection or, conversely, of the deformation degree imposed to the local airfoils in a variable geometry wing. Although there are available estimations for Δc_{lpmax} obtained with flaps deflection in literature[5],[7], the same is not true for elastically deformed wing sections.

Once this is a comparative preliminary study and there were no satisfactory airfoil analysis procedures available, it has been estimated that deformed wing sections would have, *at least*, the same c_{lpmax} performance of an airfoil equipped with plain trailing and leading edge flaps, given that the same theoretical (potential) flow deflections are observed. This measure is valid to maintain a maximum conservative philosophy. So, equivalent leading and trailing edge flap deflections are defined as illustrated in Figure 6.

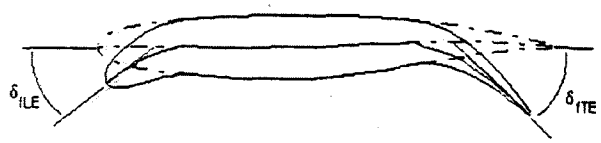

Figure 6 - Equivalent leading and trailing edge flap deflections for a deformed wing section.

Based on those hypothesis, models for c_{lpmax} variation with equivalent flap deflection δ_f have been stablished from data found in current literature[5],[6],[7]. To make final results comparable on reality basis, it has been assumed that the conventional flap analysis performed for comparison should assume high performance high lift devices, e.g. a double slotted flap and a retractable slat. From the discussion above, the following modelling equations have been assumed:

- Elastically deformable wing section:

$$c_{lpmax} = 1.7 + (2.5397\text{x}10^{-5})\,\delta_{fTE}^{3} - (7.6190\text{x}10^{-4})\delta_{fTE}^{2} + (5.0794\text{x}10^{-3})\delta_{fTE} + (0.5/30)\,\delta_{fLE} \tag{5}$$

- Double slotted flap wing section with retractable slat:

$$c_{lpmax} = 1.7 + (4.1667\text{x}10^{-5})\,\delta_{fTE}^{3} - (3.7500\text{x}10^{-3})\delta_{fTE}^{2} + \delta_{fTE}/8 + \Delta c_{lpmax,\,slat} \tag{6}$$

where: $\Delta c_{lpmax,\,slat} = 0.0$ for retracted slat;
$\Delta c_{lpmax,\,slat} = 0.5$ for deployed slat.

In the equations above, δ_{fLE} and δ_{fTE} are respectively the leading and trailing edge equivalent flap deflections given in degrees, positive as shown in Figure 6. both equations above are valid only within the ranges:

$$0 \le \delta_{fLE} \le 30.0°; \quad 0 \le \delta_{fTE} \le 40.0° \tag{7}$$

Figure 7 shows the above c_{lpmax} functions in graphic form, for trailing edge deflections. Obviously, these models are extremely simple and do not take into account Reynolds number variation, assuming an average "clean" wing $c_{lpmax} = 1.7$ for the whole wingspan. Although that approximation is not exact, the use of the same hypothesis and conservative measures for both flap and deformable wings is enough to assure initial comparisons under the same conditions.

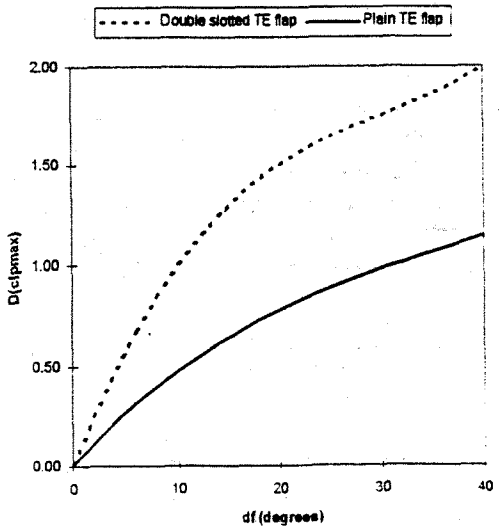

Figure 7 - Functions Δc_{lpmax} x δ_{fTE} for 25% chord double slotted and plain flaps.

Results

Figures 7 through 15 and Table 1 present several results obtained from both optimisation cases proposed in items (i) and (ii) above, for the flapped and deformable variable camber wing configurations.

Analysis of Results

Induced Drag Reduction During Takeoff and Cruise

From Figure 8 it can be observed that for the wing planform configuration studied (Figure 1), the adoption of the deformable (variable camber) wing does not bring significant induced drag reductions for C_L values between 0.2 and 1.4. Maximum reductions are observed for greater C_L values and reach the mark of 2.3% for C_L = 1.4, as seen on Figure 8.

This behaviour can be explained by Figure 12, which displays non-dimensional lift distributions of the form

$$l(y) = \frac{c_l(y)c(y)}{\text{mac.}\, C_L} \qquad (8)$$

for both the optimum deformed wing and flapped wing configurations, at minimum C_{Di} for C_L = 1.0. Also, the ideal elliptical lift distribution has been plotted against the results, for comparison. It can be observed that the flapped wing configuration already have a closely elliptical lift distribution. The variable camber wing is capable of producing an even closer to elliptical distribution, but the differences are small enough to cause no significant reduction in C_{Di}.

Maximum Lift for Landing Condition

Figure 13 shows $c_{lpmax}(y)$ and $c_l(y)$ distributions for both the flapped and the variable camber wing configurations. It can be readily observed that maximum lift for the variable camber wing remains smaller than that for a flap equipped wing, under the restrictions and hypothesis stablished above. The C_{Lmax} values obtained for both configurations are presented in Table 1.

Configuration	C_{Lmax}
Variable Camber	2.5267
Flapped wing	3.4772

Table 1 - Maximum lift coefficients (C_{Lmax}) for both optimisation proposals

It can be observed that although the variable camber wing could have the potential ability to have a $c_l(y)$ distribution which would greatly use the $c_{lpmax}(y)$ range allowed by its airfoil sections, this is not enough to reach the same C_{Lmax} performance possible with a high performance high lift configuration, *within the hypothesis and simplifications stablished before.*

Conclusion

Within the hypothesis and simplified models previously assumed for this preliminary evaluation, the following can be concluded about the comparison made between a deformable, variable wing section camber wing and a conventional wing with same basic planform, equipped with modern high lift devices:

(1) *In respect to induced drag reduction during takeoff and climb* ($0.2 \leq C_L \leq 1.4$), no significant reductions could be achieved over the conventional flapped wing by suitable wing deformation. This happens because the basic typical wing planform configuration chosen is able, by itself, of generating a highly favourable spanwise lift distribution, close to an elliptical one. As a result, lift distribution shaping by wing deformation does not bring any great improvement (Figures 7 and 11). From these facts it can be suggested, *within this study limits*, that camber elastic deformation is not advantageous for induced drag reduction on transport aircraft, which often are enabled to have wing planform configurations much more complex than the one chosen here (Figure 1).

(2) *In respect to maximum lift improvement during landing*, it can be suggested that smoothly variable camber airfoil sections *must* have significantly greater performance than plain flaps, for equivalent flap deflections (Figure 6), if any high lift performance comparable to that of modern high lift devices is to be achieved. The potential ability of spanwise deformable camber of making greater use of maximum airfoil lift by suitable spanwise $c_l(y)$ shaping is not enough to make any significant difference. To conclude any other design directive in deeper detail, wind tunnel tests and/or airfoil analysis results able to give an indication of real c_{lpmax} performance of variable camber airfoils must be available.

Once more, it is important to highlight the limiting hypothesis and simplified mathematical models used in this preliminary evaluation work. Those simplifications include considering only chordwise angles as representative of local deformation in the vortex lattice model and representing the performance of a variable camber airfoil section by equivalent deflection plain (leading and trailing edge) flaps. Although those hypothesis are useful for comparison purposes, any absolute design decision conclusion would need more exact models.

Also, it is important to be observed that no attempt to evaluate the deformable camber wing performance in respect to viscous/pressure drag has been made. The concept's potential ability to adapt the wing to have minimum viscous drag at higher C_L values is an interesting proposal for a future extension of this work.

References

[1] Siuaru, B and Busick, J. D.: *Future Flight: The Next Generation of Aircraft Technology*. TAB Books Inc., USA, 1987.

[2] Rezende, M.N. and Paiva, J.B.: *A Quadrilateral Discrete Kirchoff Finite Element for Building Slab Analysis*. In: Papadrakis, M. and Topping,B.H.V., eds. *Advances in Finite Element Techniques*. (Proc. 2nd International Conference on Computational Structures Technology, Athens, Greece, 30th Aug., 1994). Edinburgh, Civil-Comp Press, 1995. p.25-31.

[3] Megson, T.H.G.: *Aircraft Structures for Engineering Students*. Ed. Edward Arnold, UK, 1972.

[4] Martins, A.L. and Ribeiro, R.S.: *Aircraft Induced Drag Minimisation Using a Constrained Optimisation Method*. 20th Congress of the International Council of Aeronautical Sciences (ICAS 96), Italy, 1996.

[5] Torenbeek, E.: *Synthesis of Subsonic Airplane Design*. Delft University Press, The Netherlands, 1982.

[6] Hoerner, S.F.: *Fluid Dynamic Lift*. Published by the author, USA, 1975.

[7] Abbott, I.H. and Doenhoff, A.E.: Theory of Wing Sections, Ed. Dover, USA, 1959.

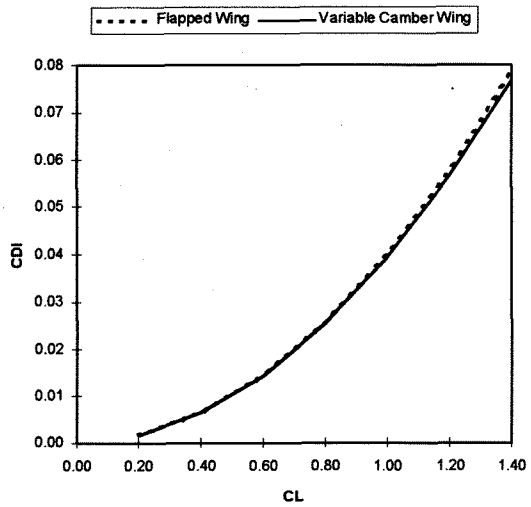

Figure 8 - $C_{Di,opt}$ x C_L curves for variable camber and flapped wing configurations.

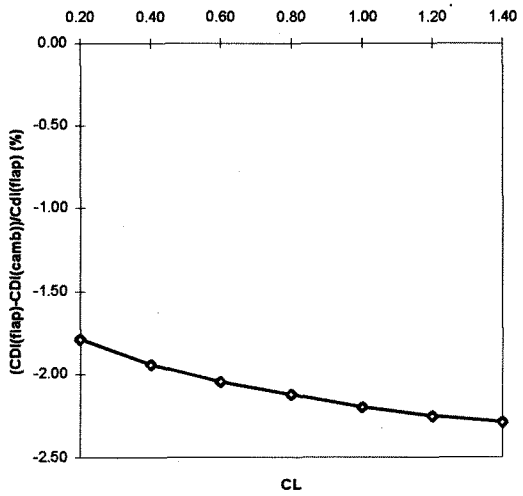

Figure 9 - Percentual decrease in C_{Di} observed for the variable camber wing in relation to the flapped wing.

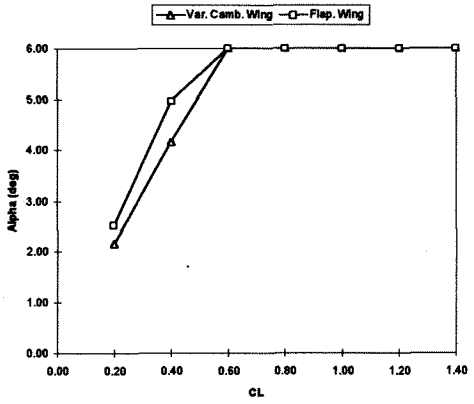

Figure 10 - Variation α x C_L observed for both flapped and variable camber wings, maximum α restricted to 6°.

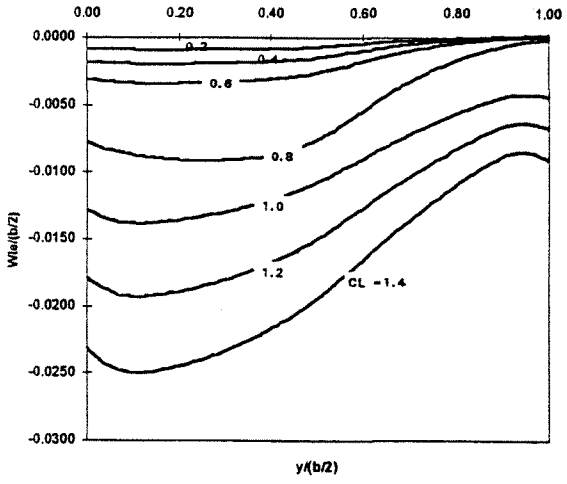

Figure 11 - Trailing edge line vertical displacements for minimum C_{Di} , variable camber, at various C_L values.

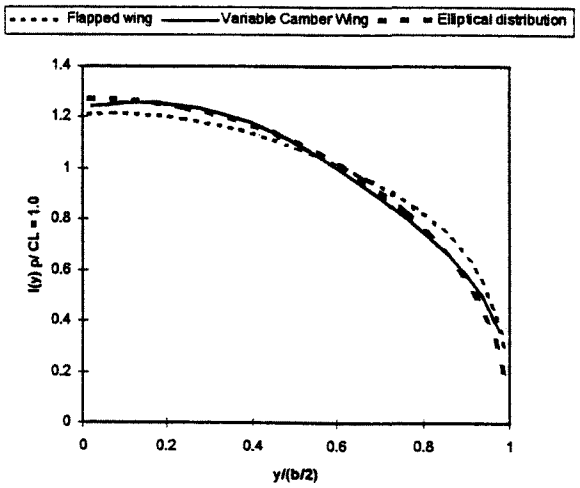

Figure 12 - Adimensional lift distributions $l(y) = c_l(y)\, c(y)/(C_L\, MAC)$ for minimum C_{Di} , at $C_L = 1.0$. Comparison with elliptical distribution.

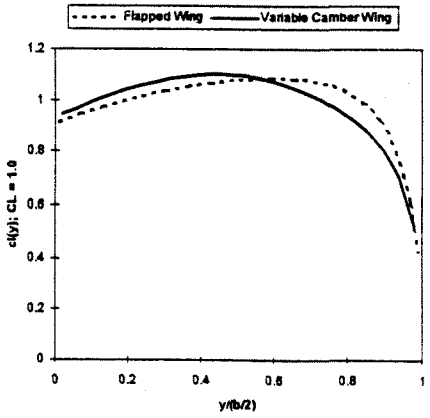

Figure 13 - Local lift coefficient distributions $c_l(y)$ for minimum C_{Di} , at $C_L = 1.0$.

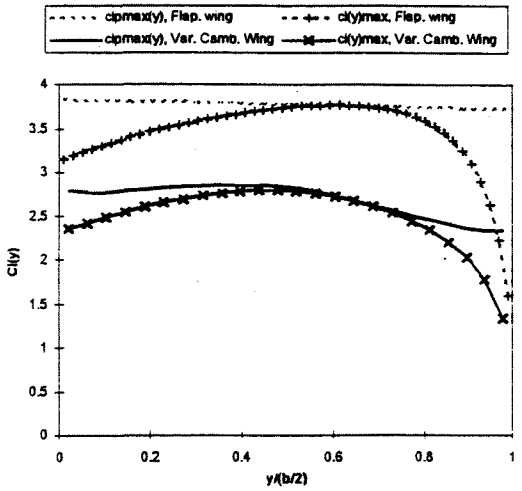

Figure 14 - Local lift coefficient distributions $c_l(y)$ and maximum airfoil lift coefficients $c_{lpmax}(y)$ at $C_L = C_{Lmax}$.

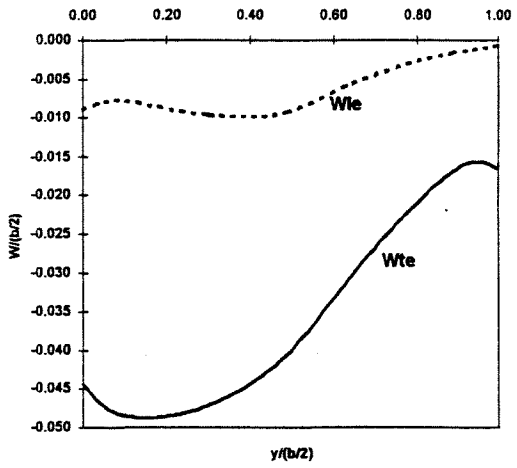

Figure 15 - Trailing and leading edge line vertical displacements for $C_L = C_{Lmax}$, variable camber.

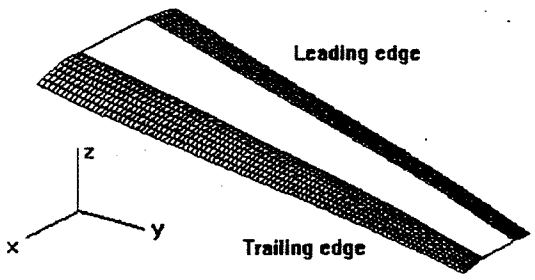

Figure 16 - Three-dimensional representation of the variable camber wing mean surface for $C_L = C_{Lmax}$ (only half wing shown; axis directions indicated)